

XMM-NEWTON OBSERVATIONS OF NGC 247: X-RAY POPULATION AND A SUPERSOFT ULTRALUMINOUS X-RAY SOURCE

JING JIN¹, HUA FENG¹, PHILIP KAARET², SHUANG-NAN ZHANG³

Accepted for publication in The Astrophysical Journal

ABSTRACT

We report on a new XMM-Newton observation of NGC 247 from December 2009. The galaxy contains a supersoft, ultraluminous X-ray source (ULX) whose spectrum consists of a thermal component with a temperature about 0.1 keV and a power-law tail with a photon index around 2.5. The thermal emission is absolutely the dominant component, contributing 96% of the total luminosity in the 0.3-10 keV band. Variability is detected at timescales of 10^2 s and longer with a ν^{-1} power spectrum. These properties are consistent with black hole binaries in the thermal state and suggest the presence of an intermediate mass black hole of at least 600 solar masses. However, the integrated rms power is much higher than typically found in the thermal state. An alternative explanation of the emission could be a photosphere with a radius about 10^9 cm. A possible absorption feature around 1 keV is detected, which may be due to absorption of highly ionized winds. X-ray sources within the disk of NGC 247 have a luminosity function consistent with that found in low mass X-ray binaries. We confirm previous results that X-rays from the quasar PHL 6625 may be absorbed by gas in NGC 247, mainly at energies below 0.3 keV.

Subject headings: X-rays: galaxies — X-rays: binaries — black hole physics — accretion, accretion disks — galaxies: individual (NGC 247)

1. INTRODUCTION

Nonnuclear X-ray sources with luminosities higher than 3×10^{39} erg s⁻¹ are classified as ultraluminous X-ray sources (ULXs). Many of them are variable and most likely powered by accretion onto black holes. However, their luminosities, assuming isotropic emission, are higher than the maximum seen in Galactic black hole binaries, suggesting the presence of intermediate mass black holes with masses of $10^2 - 10^4 M_{\odot}$ (Colbert & Mushotzky 1999; Kaaret et al. 2001; Farrell et al. 2009) or super-Eddington accretion onto stellar mass black holes of about $10 M_{\odot}$ (Watarai et al. 2001; Begelman 2002). Discovery of intermediate mass black holes would be important because they cannot be formed via core collapse of a single star with normal metallicity (Belczynski et al. 2010) and may shed light onto the formation of supermassive black holes in the early Universe (Ebisuzaki et al. 2001; Volonteri 2010).

Dynamical measurement of the compact object mass for ULXs has been unfeasible to date (Roberts et al. 2010). Instead, indirect means such as X-ray spectroscopy may shed light on the black hole mass. At a fixed Eddington ratio, the inner temperature of the accretion disk scales with black hole mass as $T_{\text{in}} \propto M^{-1/4}$ (Makishima et al. 2000). Application of this relation requires the black hole binary to be in the thermal state (McClintock & Remillard 2006; Remillard & McClintock 2006), in which the disk is believed to extend all the way to the last stable orbit around

the black hole. However, the thermal state is rarely found in ULXs, the only known occurrences are M82 X41.4+60 (Feng & Kaaret 2010) and M82 X37.8+54 (Jin et al. 2010) during outburst. X-ray sources with soft, $kT_{\text{in}} \sim 0.1$ keV, thermal spectra may be good candidates for intermediate, $\sim 10^3 M_{\odot}$, mass black holes in the thermal state.

NGC 247 is a nearby spiral galaxy in the Sculptor Group, with a modest star formation rate estimated to be about $0.1 M_{\odot} \text{ yr}^{-1}$ by counting bright main-sequence stars (Davidge 2006) or based on H α observations (Ferguson et al. 1996). However, infrared and radio observations suggest a star formation rate 10 or 100 times lower (Davidge 2006). The distance to NGC 247 has been measured independently by different groups using various means. Among them, the recent result from Gieren et al. (2009) using near-infrared observations of Cepheids is claimed to be the most accurate. We therefore adopt that distance of 3.4 Mpc in this paper.

Previously, NGC 247 has been observed in the X-ray band with Einstein (Fabbiano et al. 1992), ROSAT (Zang et al. 1997; Read et al. 1997; Lira et al. 2000), and XMM-Newton (Winter et al. 2006). A bright, off-nucleus X-ray source (NGC 247 ULX = 1RXS J004704.8–204743) was detected in all of these observations. ROSAT observations revealed a very soft spectrum with $kT = 0.12$ keV (Read et al. 1997). Later on, the source was observed to have brightened by a factor of 2 (Lira et al. 2000), suggestive of an accretion powered system. In 2001, XMM-Newton detected the source at the highest flux observed to date, with an unabsorbed luminosity of 8×10^{39} erg s⁻¹ (at 3.4 Mpc) in the 0.3-10 keV band, and the spectrum was still dominated by a soft thermal component with $kT = 0.12$ keV (Winter et al. 2006).

These results imply that the source is a good candidate

¹Department of Engineering Physics and Center for Astrophysics, Tsinghua University, Beijing 100084, China

²Department of Physics and Astronomy, University of Iowa, Van Allen Hall, Iowa City, IA 52242, USA

³Key Laboratory of Particle Astrophysics, Institute of High Energy Physics, Chinese Academy of Sciences, Beijing 100049, China

to be an intermediate mass black hole in the thermal state. Unfortunately, the 2001 XMM-Newton observation suffered strong background flares, resulting in little usable data and poor statistics in the extracted spectrum. Thus, we proposed a new XMM-Newton observation of NGC 247 to obtain a better spectral measurement. In this paper, we report results from the new observation about the ULX as well as other sources in NGC 247.

2. OBSERVATIONS AND RESULTS

The observation was performed on 2009 Dec 27 (PI: H. Feng), lasting about 35 ks, with the prime full window for the three cameras. The thin filter was chosen for the PN and medium filter for the MOS. Event lists were created from the observation data files using SAS with recent calibrations. To minimize background contamination, we selected good time intervals (GTIs) where the 10-15 keV count rate of the whole CCD was lower than the 3σ upper limit of the quiescent level. This resulted in 22 ks of clean exposure for the PN and 30 ks for the MOS.

Images in two energy bands, 0.3-2 keV and 2-10 keV, were created for each CCD with a pixel size of $4.1''$ from events with FLAG = 0 and PATTERN ≤ 4 for the PN or PATTERN ≤ 12 for the MOS. The `edetect_chain` tool was used to detect point sources simultaneously on the six images. A total number of 75 sources with likelihood ($= -\ln(p)$, where p is the chance probability) over 10 were detected and are listed in Table 1 and shown in Figure 1. The astrometry was corrected by aligning the X-ray position of the known quasi-stellar object (QSO) PHL 6625 (source 22) to its optical position quoted in the USNO-B1.0 catalog.

The absorbed flux of each source was calculated from the net counts and an effective exposure with a response matrix created at the source position on the CCD assuming a power-law spectrum with Galactic absorption ($N_{\text{H}} = 2.01 \times 10^{20} \text{ cm}^{-2}$; Kalberla et al. 2005) and a photon index of 1.7. We note that this is more accurate than using a single conversion factor in `edetect_chain` as the energy band is wide. In the calculation, either the PN or the averaged MOS count rate was adopted depending on which likelihood was higher. For sources 38, 60, and 63, only the MOS2 data was adopted as they were not covered by the MOS1. The hardness ratio was calculated using `edetect_chain` for each source as $(R_2 - R_1)/(R_2 + R_1)$, where R_1 and R_2 are vignetting-corrected net count rates in the soft and hard bands, respectively.

For 15 sources, optical or infrared sources in the USNO-B1.0 or Two Micron All Sky Survey catalogs are found in a $2''$ -radius circle around their corrected X-ray positions, and are indicated in Table 1. Most of the sources with optical/IR counterparts, 11 out of 15, are outside of the D25 ellipse of NGC 247.

For sources with 200 or more net counts, we extracted the PN and the MOS spectra and fitted them simultaneously with a power-law model subject to interstellar absorption. The lower limit of the absorption column density was set to the Galactic value. For sources 4 and 67, only the MOS spectra were adopted as they lie on a gap or bad pixels on the PN. For PHL 6625, only the PN data were adopted for the same reason, and a redshifted

power-law model with $z = 0.38$ was used.

The best-fit spectral parameters are listed in Table 2, except for the ULX. Among them, seven sources (4, 16, 19, 22, 39, 61, and 62) are coincident with an optical counterpart in USNO-B1.0, and source 67 has two possible counterparts. We calculated their X-ray to optical flux ratios as $\log(f_{\text{X}}/f_{\text{V}}) = \log f_{\text{X}} + m_{\text{V}}/2.5 + 5.37$, where f_{X} is the observed flux in the 0.3-3.5 keV band in units of $\text{erg cm}^{-2} \text{ s}^{-1}$ and m_{V} is the visual magnitude (Maccacaro et al. 1982). The average of the second red and blue magnitudes in USNO-B1.0, if available, was used to estimate the visual magnitude, otherwise, the red or blue magnitude is taken as an approximation to m_{V} . The X-ray to optical flux ratios are 0.52, 0.05, 0.24, 0.33, -0.28 , -0.26 , 0.04, respectively for sources 4, 16, 19, 22 (PHL 6625), 39, 61, 62. For source 67, the ratio is 0.20 or 0.54 depending on the counterpart. These values are consistent with those found for active galactic nuclei (AGN) and clusters of galaxies (Maccacaro et al. 1988; Stocke et al. 1991); the ratios for sources 39 and 61 are also consistent with those of normal galaxies, and the ratios for source 4 and source 67 (with the dimmer optical counterpart) are also consistent with those of BL Lac objects.

For other sources that are associated with an optical counterpart but do not have enough photons for spectral fitting, we calculated their 0.3-3.5 keV fluxes from count rates and the X-ray to optical flux ratios were found in a range from -2.2 to -0.2 , which are consistent with those of AGN or normal galaxies, but smaller than those of X-ray binaries. Two of them (source 48 and source 57 with the brighter optical counterpart, both in D25) with ratios smaller than -1.5 could also be foreground M or K dwarfs in the halo of the Milky Way. Thus, we conclude that sources associated with bright optical sources are unlikely to be members of NGC 247, and more likely to be background or foreground objects.

The cumulative X-ray luminosity function (XLF) for sources inside the D25 ellipse of NGC 247 is plotted in Figure 2. For sources with enough photons, those in Table 2 and the ULX, the flux in the 0.3-10 keV band from spectral fitting is adopted, otherwise, the two fluxes in Table 1 after correction for Galactic absorption are summed and adopted. For comparison, two model XLFs are shown. The shallower curve is the XLF expected for high mass X-ray binaries (HMXBs): a power-law with a slope of -0.61 as found for HMXBs in nearby starburst galaxies normalized to a star formation rate of $0.1 M_{\odot} \text{ yr}^{-1}$ (Grimm et al. 2003; Davidge 2006; Ferguson et al. 1996). The steeper curve is the XLF for low mass X-ray binaries (LMXBs), a power-law with a slope of -1.1 (Kim & Fabbiano 2004), normalized to the observed number of sources at $L_{\text{X}} > 10^{38} \text{ erg s}^{-1}$. Comparing the curves with the data, it is clear that the X-ray binary population in NGC 247 is dominated by LMXBs.

For sources outside of the D25 ellipse, we plotted $\log N(> S)$ versus $\log S$, where S is the observed flux in the 2-8 keV band and $N(> S)$ is the number of sources with flux greater than S , see Figure 3. For comparison, we show a power-law index of -1.6 as expected for AGN (Brandt & Hasinger 2005). The power-law is normalized to a solid angle of 0.16 degree^2 , equal to the sky area outside the D25 ellipse of NGC 247 and in the field of

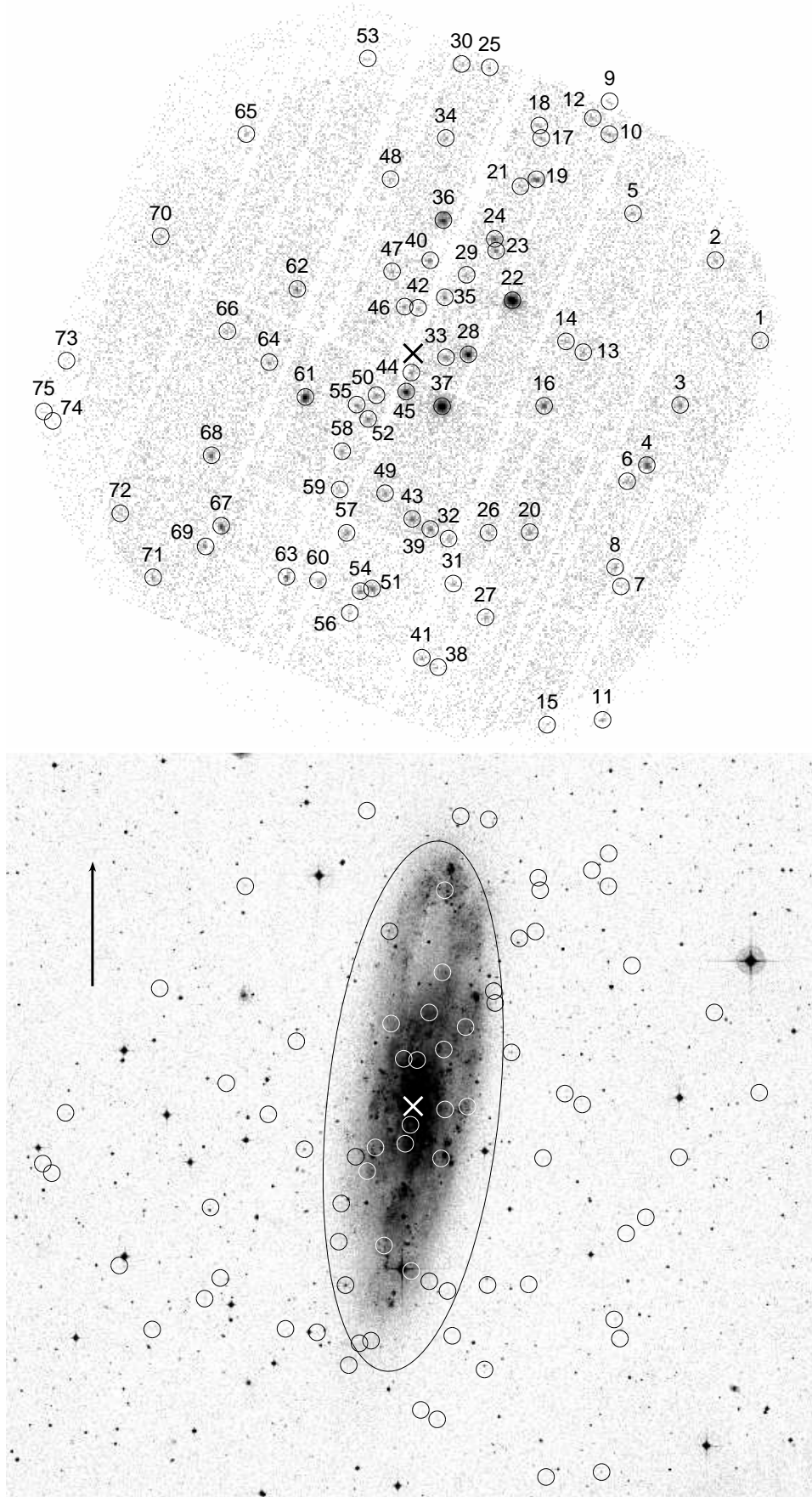


FIG. 1.— X-ray (left) and optical (right) images of NGC 247. The X-ray image is created from the combined PN and MOS data and circles indicate detected sources. Source 22 is PHL 6625 and source 37 is the ULX. The cross indicates the galaxy center. The optical image is from the Digitized Sky Survey blue band and the ellipse indicates the D25 region of NGC 247. The arrow points north and has a length of $5'$.

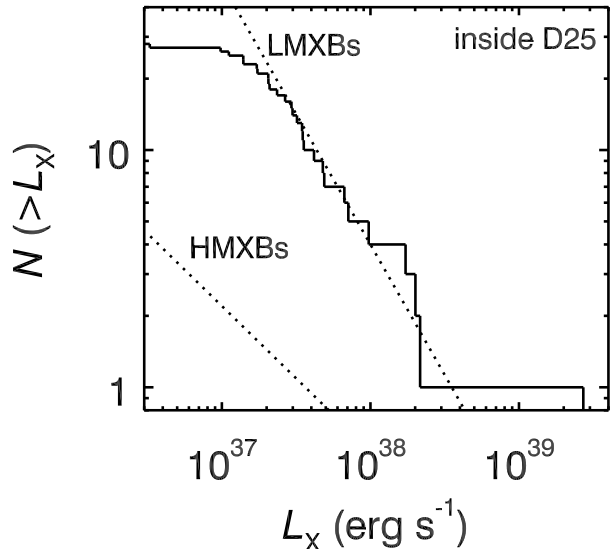


FIG. 2.— Cumulative X-ray luminosity functions of NGC 247 for sources inside the D25 ellipse. The steep dotted line is the luminosity function for LMXBs with a slope of -1.1 normalized to the observed number at 10^{38} erg s^{-1} . The shallower dotted line is the luminosity function for HMXBs with a slope of -0.61 normalized to a star formation rate of $0.1 M_{\odot} \text{ yr}^{-1}$.

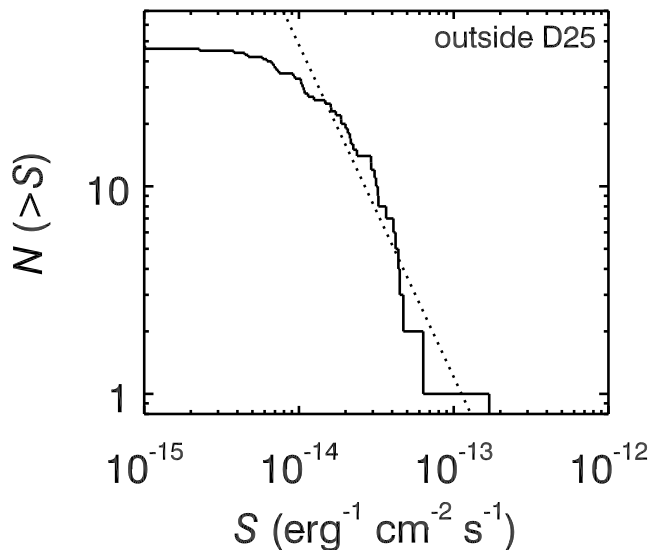


FIG. 3.— Number of sources, $N(> S)$, brighter than a given observed flux in the 2-8 keV band, S , for sources outside of the D25 ellipse of NGC 247. The dotted line is the distribution for AGN with a slope of -1.6 normalized to the observed solid angle of about 0.16 degree^2 .

view of XMM-Newton.

We examined short-term variability for each source using photons in the 0.3-10 keV band with the Kolmogorov-Smirnov test. Only the ULX shows evidence for variability with a chance probability lower than 10^{-3} .

2.1. Spectral and timing analysis of the ULX

Due to the soft spectrum of the ULX and the thin filter on the PN, the number of photons detected on the PN is about 3-4 times that on each MOS. Thus, we used only the PN data for spectral analysis. The energy spectrum was extracted from events in a $30''$ -radius circular

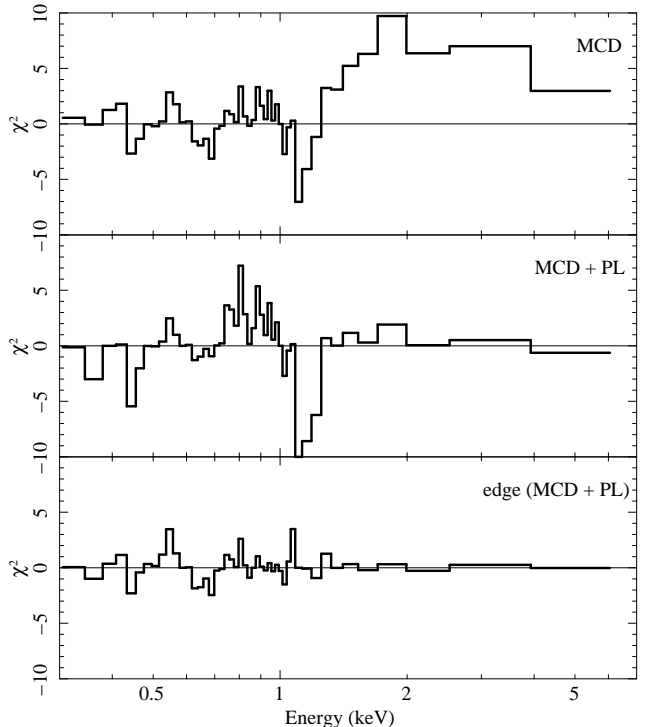


FIG. 4.— Residuals in units of χ^2 from fits to the spectrum of NGC 247 ULX with models $\text{wabs} * \text{diskbb}$, $\text{wabs} * (\text{diskbb} + \text{powerlaw})$, $\text{wabs} * \text{edge} * (\text{diskbb} + \text{powerlaw})$, respectively.

region around the source to avoid CCD gaps and with FLAG and PATTERN the same as those used in creating the image. Background was subtracted from events in a nearby circular region with a radius of $45''$ on the same CCD and off the readout column of the ULX. To avoid spurious spectral structure caused by over-sampling of the spectrum, the energy channels were grouped with a bin size of $1/5$ th of the local spectral resolution (in terms of full width at half maximum) and to have at least 15 net counts per bin.

A single power-law subject to interstellar absorption is inadequate to fit the ULX spectrum, resulting in $\chi^2 = 198.0$ for 44 degrees of freedom (dof). An absorbed multicolor disk (MCD) model provides a better fit with $\chi^2/\text{dof} = 98.5/44$, but is still inadequate, especially at energies above 1.4 keV where a hard excess is obvious, see the top panel in Figure 4. Therefore, we used a model with the sum of a power-law and a MCD, which significantly improved the fit with $\chi^2/\text{dof} = 63.4/42$. To test the significance of the power-law tail, we simulated 10^4 spectra based on the single MCD model. In none of the simulated spectra did addition of a power-law reduce the χ^2 by the amount seen in the real data. This suggests a chance probability less than 10^{-4} . The F-test gives a consistent probability of 9.5×10^{-5} despite caveats about its validity in such a case (Protassov et al. 2002).

Although the MCD plus power-law model improves the fit considerably, it still does not provide an adequate fit. As one can see from the middle panel of Figure 4, most residuals arise around 1 keV and appear like an absorption feature. Thus, we then tried two absorption components, both of which gave adequate fits. An absorption edge at 1.02 keV gave $\chi^2/\text{dof} = 36.8/40$ and

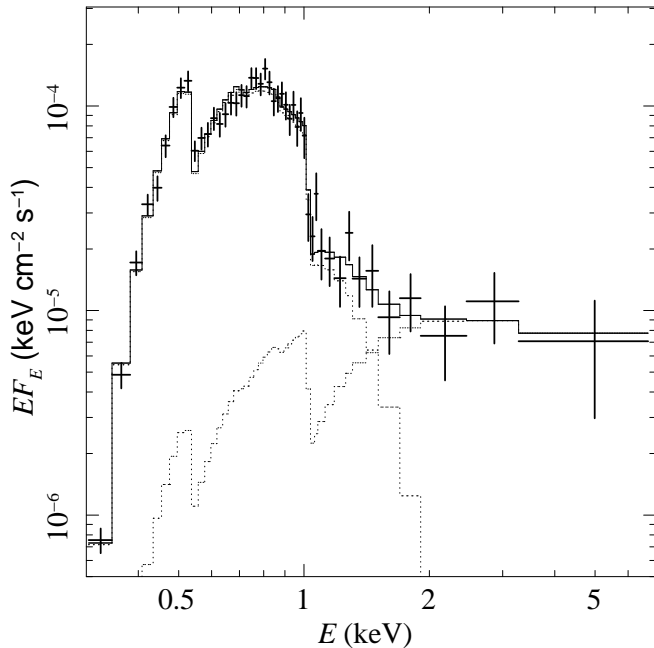


FIG. 5.— The unfolded spectrum of NGC 247 ULX fitted with the MCD plus power-law model with edge and interstellar absorption.

a Gaussian absorption line with a centroid of 1.16 keV gave $\chi^2/\text{dof} = 37.0/39$. The residuals for both models are flat throughout the passband, see the bottom panel of Figure 4. The absorption equivalent width is 0.13 to 0.19 keV, depending on the model. Similarly, we tested the significance of the absorption component using simulations, and an edge was detected as significant in only 1 out of 10^4 trails, indicative of a chance probability of $\sim 10^{-4}$.

The spectral parameters are listed in Table 3. Due to the poor fit of the MCD plus power-law model, we fixed the absorption column density at the best value, $N_{\text{H}} = 3.2 \times 10^{21} \text{ cm}^{-2}$, obtained from the best-fit model. Consistent parameters of the continuum components were obtained for all models. The unfolded spectrum from the MCD plus power-law model with absorption edge is plotted in Figure 5. The MCD is the dominant component of the spectrum, with a contribution of 96% of the total unabsorbed flux in the 0.3-10 keV band.

We also replaced the MCD with a blackbody and obtained similar results as shown in Table 3. We note that the use of a more sophisticated model for interstellar absorption, such as `tbabs`, leads to almost identical results as obtained with `wabs` due to the moderate resolution and statistics.

We tried to fit the spectrum with a MCD plus Comptonization model, which is found to fit for ULX spectra with high statistics (Gladstone et al. 2009). This model provides an equally good fit as the MCD plus power-law model and results in almost identical parameters for the disk component. The disk temperature is $0.13 \pm 0.02 \text{ keV}$ and the inner disk radius is $0.9^{+0.9}_{-0.5} \times 10^4 \text{ km}$ assuming a face-on orientation. A similar edge is required in the model at $1.02^{+0.02}_{-0.03} \text{ keV}$, with optical depth of $1.4^{+0.5}_{-0.2}$. The Comptonization parameters are poorly constrained due to the low number of photons in the 2-10 keV band.

Light curves of the ULX were created using the PN

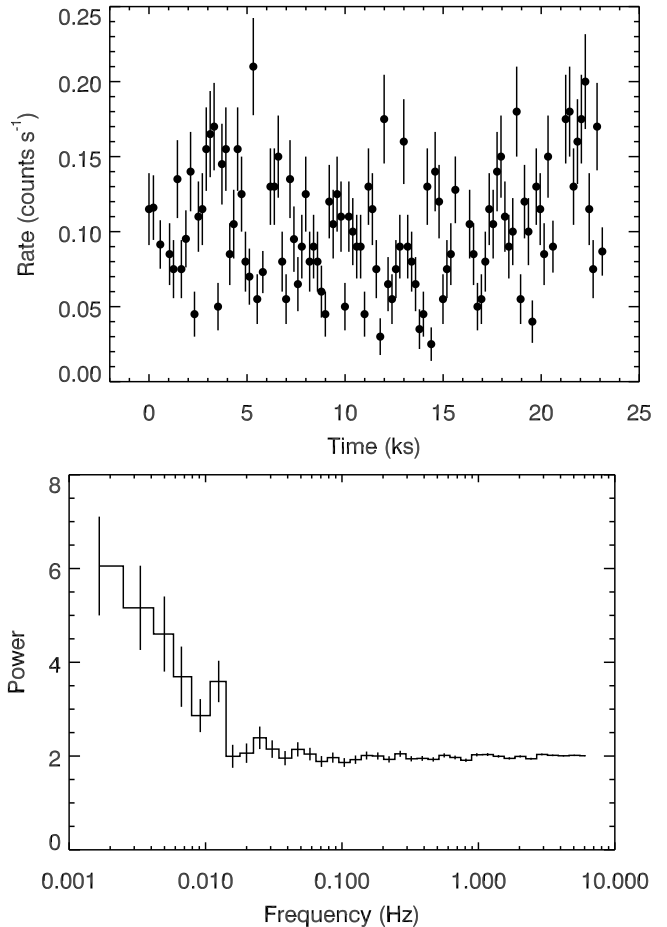


FIG. 6.— X-ray lightcurve and power spectrum of NGC 247 ULX in the energy range of 0.3-2 keV. The lightcurve has a time bin size of 200 s.

events in the same region as for spectral analysis with `FLAG = #XMMEA_EP` and `PATTERN ≤ 4` . Continuous intervals with low background were selected from within the GTIs. The 0.3-2 keV light curve shown in Figure 6 has a bin size of 200 s.

For each continuous interval, power spectra were calculated from a light curve with a bin size equal to the CCD frame time, $\sim 73 \text{ ms}$, using 8192-point Fourier transforms. A final power spectrum was created by averaging all the individual power spectra with frequency channels geometrically binned by a factor of 1.2. Each point in the final spectrum is the mean of at least 33 individual data points, to assure validity in modeling the spectrum using minimal χ^2 . The final power spectrum in the 0.3-2 keV band normalized following Leahy et al. (1983) is shown in Figure 6. A power-law plus a constant can adequately fit the power spectrum, with the constant describing the Poisson noise level of 1.995 ± 0.009 and the power-law describing low-frequency noise with a slope of $1.22^{+0.20}_{-0.16}$. The source count rate is $0.10 \text{ counts s}^{-1}$ in the 0.3-2 keV band and the background photon fraction is estimated to be 4.1%. The fractional root-mean-square (rms) power of the source is estimated to be 0.52 by integrating the power-law component over 0.001-0.1 Hz, or 0.31 extrapolating the power-law to the frequency range 0.1-10 Hz. The power spectrum in the 2-10 keV band is consistent

with that of Poisson noise, due to poor statistics.

We re-analyzed the XMM-Newton observation of NGC 247 obtained in 2001 in a similar way. As the background is too high to find a quiescent level adaptively for the PN data, an additional requirement that the background count rate is less than $1.5 \text{ counts s}^{-1}$ for the PN is imposed to generate GTIs. The PN and the MOS spectra are fitted simultaneously with a MCD plus power-law model, resulting in $\chi^2/\text{dof} = 53.4/49$. The MCD component contributes about 88% of the unabsorbed luminosity in the 0.3-10 keV band, which is $L_X = 8^{+13}_{-4} \times 10^{39} \text{ erg s}^{-1}$, with a disk inner temperature of $0.15 \pm 0.03 \text{ keV}$ and a face-on inner radius of $1.2^{+2.5}_{-0.7} \times 10^4 \text{ km}$. The photon index of the power-law component is poorly constrained, with a 90% upper limit of 3.8. The interstellar absorption has a column density of $3.6^{+1.3}_{-1.0} \times 10^{21} \text{ cm}^{-2}$. The best-fit parameters are consistent with those reported in Winter et al. (2006) within errors.

3. DISCUSSION AND CONCLUSION

3.1. X-ray population in NGC 247

The XMM-Newton observation of NGC 247 obtained in December 2009 is, to date, the deepest X-ray observation of the galaxy and allows an X-ray source population study. As shown in Figure 2, sources inside the D25 ellipse of NGC 247 have a luminosity function well consistent with that of LMXBs. A population of X-ray sources dominated by LMXBs is reasonable given the low star formation rate of the galaxy.

For sources outside of the D25 ellipse of the galaxy, the $\log N(> S)$ versus $\log S$ distribution is roughly consistent with that expected for AGN (Brandt & Hasinger 2005) (Figure 3) at fluxes above $2 \times 10^{-14} \text{ erg cm}^{-2} \text{ s}^{-1}$. Below this flux, the distribution flattens significantly with decreasing flux. This may be caused by the decrease of sensitivity due to vignetting at large off-axis angles. Some of these sources have bright optical counterparts with an X-ray to optical flux ratio consistent with that of AGN. Therefore, we conclude that most sources outside of the D25 ellipse of NGC 247 are likely background objects.

3.2. NGC 247 ULX

The observed X-ray spectrum of the ULX is completely dominated by a cool, thermal emission component with a temperature around 0.1 keV; a weak power-law tail with a photon index of about 2.5 is also evident but contributes only a small fraction of the flux. This spectral shape is in contrast with that of many other ULXs whose high energy component contributes the majority of the flux (more than 60%) and can be explained by an optically-thick corona (Gladstone et al. 2009). In fact, Gladstone et al. (2009) fits can predict an intrinsically soft-dominated spectrum, but this is a model-dependent result, while the observed spectral shapes of their sources are always dominated by the emission from a hard tail. It is unlikely that the high energy component in NGC 247 ULX arises from an optically thick corona; otherwise, such a corona must have a tiny covering factor since most disk photons are unscattered.

The spectrum, however, is consistent with that of black hole binaries in the thermal state (McClintock & Remillard 2006;

Remillard & McClintock 2006), and may hint at a reconnection in nature. An important observational characteristic of the thermal state is that the disk luminosity varies roughly with the 4th power of the disk inner temperature, equivalent to a constant disk inner radius. This source has shown a consistent disk inner radius derived from two XMM-Newton observations, though the constraint from the 2001 observation is loose. For a positive identification of the thermal state, one also needs timing information. This ULX displays red noise with a ν^{-1} form above the white noise, which is consistent with that seen in the thermal state. However, the integrated rms power is significantly higher than that seen in the thermal state. For Galactic black holes, the total rms power in the 0.1-10 Hz band is usually less than 0.075 in the thermal state, and only in the hard state is the rms power found to be greater than 0.15 (Remillard & McClintock 2006). However, the X-ray spectrum of the ULX is much too soft to be classified as in the hard state.

If the ULX is in the thermal state, then the source would be an interesting candidate to be an intermediate mass black hole. The accretion disk in the thermal state is believed to extend all the way to the innermost stable circular orbit (ISCO) around the central black hole. The ISCO radius depends only on the black hole mass and spin, as $R_{\text{ISCO}} = 6GM/c^2$ for a non-spinning black hole or 6 times smaller for an extremely spinning object, where G is the gravitational constant, M is the black hole mass, and c is the light speed. Assuming a hardening correction of 1.7 and that the maximum temperature occurs at 2.4 times the ISCO radius (Makishima et al. 2000), the ISCO radius can be expressed as $R_{\text{ISCO}} \approx 1.2R_{\text{in}}$, where R_{in} is the apparent inner radius derived directly from the normalization of the MCD component. Adopting the parameters from the best-fitted model, MCD plus power-law with absorption edge, and assuming a face-on disk, we have $R_{\text{in}} = (0.5 - 2.2) \times 10^4 \text{ km}$ in the 90% confidence region, corresponding to the ISCO radius of a $600 - 3000M_{\odot}$ Schwarzschild black hole, or a more massive black hole if spinning or the disk is tilted. The observed luminosity is about a few percent of the Eddington limit of such a black hole, which is consistent with Eddington ratios typically found in the thermal state. Similar results can be obtained with the Gaussian absorption line.

Due to the lack of a characteristic feature in the power spectrum, we are unable to constrain the black hole mass via timing. The rms-mass relation derived for AGN (Zhou et al. 2010) may have issues in extrapolation to lower masses. The faintness in the 2-10 keV band of the source prevents us from implementing the means proposed by González-Martín et al. (2011) to estimate the black hole mass.

A few other ULXs show a dominant soft, thermal emission component, and are classified as supersoft ULXs: M101 ULX-1 (Pence et al. 2001; Kong et al. 2005; Mukai et al. 2005), Antennae X-13 (Fabbiano et al. 2003), M81 ULS1 (Swartz et al. 2002; Liu 2008), and NGC 4631 X1 (Carpano et al. 2007; Soria & Ghosh 2009). These sources also show extreme variability: the observed fluxes vary by up to a factor of a few tens, and the intrinsic luminosity changes may be as large as factors of $10^2 - 10^3$ (Kong et al. 2004; Mukai et al. 2005;

Liu 2008). Short-term variability has been detected in almost all of these sources at timescales down to a few ks (Swartz et al. 2002; Mukai et al. 2005; Carpano et al. 2007; Liu 2008). M101 ULX-1 also showed a power spectrum with a ν^{-1} form at frequencies below 10^{-3} Hz (Mukai et al. 2005) during its outburst in 2000 March with variability more pronounced at high energies (0.8-2 keV) than in the lower band (0.2-0.8 keV) (Mukai et al. 2003). For a direct comparison, we calculated the rms power of NGC 247 ULX in the same energy bands and found that the fractional rms is 0.80 in the 0.8-2 keV band and 0.44 in the 0.2-0.8 keV band. Similar to NGC 247 ULX, NGC 4631 X1 also exhibits an absorption edge at 1.01 keV with an optical depth of 2.0 in its high state (Soria & Ghosh 2009). These similarities suggest that NGC 247 ULX may be a new member of the supersoft, ultraluminous family.

The other soft ULXs seem to keep a constant temperature during huge changes in luminosity, indicative of a dramatic change of the emitting surface area of the same order. Fabbiano et al. (2003) has pointed out that this would lead to difficulty in interpreting the emission as due to accretion power release within a few Schwarzschild radii of the black hole. For NGC 247 ULX, the four ROSAT and two XMM-Newton observations have detected a change by a factor of about 3 of the observed flux in 0.1-2 keV, which is significantly smaller than others. Therefore, the thermal state interpretation has not been ruled out for NGC 247 ULX; new, multiple observations are the key to revealing its nature.

An alternative explanation of the soft, thermal emission is that it arises from a photosphere that has a radius of 10^9 cm, inferred from the blackbody component. The shortest timescale of variation above white noise is about 10^2 s (Figure 6), which places a constraint that the emitting area must be smaller than 10^{12} cm, compatible with the size obtained from the blackbody parameters. This photosphere is unlikely the surface of a white dwarf, as the observed luminosity and temperature are too high to be explained by steady nuclear burning on a white dwarf surface (Starrfield et al. 2004). Plus, presence of the power-law component with a 0.3-10 keV luminosity of 1.2×10^{38} erg s $^{-1}$ is unexpected in such a case. It has been suggested that supercritical accretion could drive massive outflows above the disk and form an optically-thick photosphere, with a temperature expected to be about 0.1 keV, which could shield the inner disk emission when viewed at a high inclination angle (Ohsuga et al. 2005; Poutanen et al. 2007). In this picture, the supersoft ULXs and normal ULXs are the same objects with different viewing angles. This interpretation may be in accord with the absorption feature observed at ~ 1 keV, which is likely due to L shell transitions of highly ionized iron. Besides this ULX and NGC 4631 X1, less similar absorption features near this energy have been detected in the ULX NGC 1365 X1 (Soria et al. 2007) and in the quasar PDS 456 (Reeves et al. 2003), and are explained as a spectral signature of a massive outflow. The absence of absorption from low-Z elements like oxygen could be a consequence of high ionization.

We conclude that the X-ray properties of the NGC 247 ULX are unlike any popular emission state known in black hole binaries. The source exhibits a spectrum like

the thermal state, but shows variability much stronger than seen in the thermal state. A possible strong absorption feature is detected. This source and other supersoft ULXs may exhibit a new accretion state that is different from those seen in Galactic black hole binaries and the majority of ULXs.

A variety of potential thermal emission components have been suggested to be present in the energy spectrum of ULXs, including the soft excess (0.1-0.4 keV) found in the majority of ULXs (Feng & Kaaret 2005; Stobbart et al. 2006), the high-temperature (\sim keV) ULXs (Makishima et al. 2000), and supersoft ULXs. The properties of these thermal components are summarized and compared in Table 4, with NGC 247 ULX and M82 X41.4+60 in the thermal state highlighted. Among them, a disk interpretation is best established for M82 X41.4+60 because its thermal state is consistent with those of stellar-mass X-ray binaries in terms of timing and spectral properties and spectral evolution (Feng & Kaaret 2010). For the others, definitive evidence is lacking for positive determination of their nature, except that the disk explanation is ruled out for other supersoft ULXs other than NGC 247 ULX. Based on the timing information, it appears unlikely that the soft excess in 'normal' ULXs and the soft (dominant) spectral component in supersoft ULXs have the same physical origin.

3.3. PHL 6625

PHL 6625 was identified as a radio-quiet background QSO at $z = 0.38$ based on a Mg II emission line (Margon et al. 1985). A single power-law model with interstellar absorption provides an adequate fit to its X-ray spectrum. The parameters listed in Table 2 are obtained from fitting in the 0.3-10 keV energy range, and the hydrogen column density is very close to the Galactic value at $N_{\text{H}} = 2 \times 10^{20}$ cm $^{-2}$, indicative of negligible absorption within NGC 247. However, if we include data down to 0.2 keV, two more energy bins, then the best-fit absorption is $N_{\text{H}} = 5.3_{-1.0}^{+1.2} \times 10^{20}$ cm $^{-2}$. This is caused by the low flux between 0.2-0.3 keV, and is consistent with the results obtained from ROSAT observations, in which a total absorption column density $N_{\text{H}} = 5.4_{-2.1}^{+2.4} \times 10^{20}$ cm $^{-2}$ was derived from fitting in the 0.1-2 keV band, and the excess absorption mainly takes effect at energies below 0.3 keV (Elvis et al. 1997). Those authors claimed a positive detection of absorbing materials in NGC 247 assuming a Galactic $N_{\text{H}} = 1.4 \times 10^{20}$ cm $^{-2}$ based on 21 cm observations of neutral hydrogen. Here, we confirm this conclusion with tighter constraints, even assuming a higher Galactic absorption. Therefore, with future high-resolution spectroscopic observations, this QSO could be used to study the interstellar medium within NGC 247.

For the 2009 data, the power-law photon index at the rest frame is $\Gamma = 2.10_{-0.09}^{+0.13}$. We extracted spectra for this object from the 2001 XMM-Newton observation and found a harder spectrum with $\Gamma = 1.64 \pm 0.17$ at a flux level of $3.7 \pm 0.6 \times 10^{-13}$ erg cm $^{-2}$ s $^{-1}$ in 0.3-10 keV similar to that in 2009. The fluxes observed with XMM-Newton are about ten times lower than the ROSAT flux of $(5.9 \pm 0.7) \times 10^{-12}$ erg cm $^{-2}$ s $^{-1}$ in the 0.2-2.4 keV band (Elvis et al. 1997). No short-term X-ray variability

has been detected for this object.

3.4. Other individual sources

Source 28. — The source is hard, and its spectrum can be described by a power-law with $\Gamma = 1.27$, but the residuals vary systematically with energy. Adding an MCD component improves the residuals and results in $\chi^2/\text{dof} = 31.7/54$. The disk has a temperature at the inner radius of $0.35_{-0.10}^{+0.14}$ keV with a bolometric luminosity of 2×10^{37} erg s $^{-1}$ assuming a face-on geometry, and the power-law component has a photon index $\Gamma = 0.6_{-0.3}^{+0.2}$. The disk component has a fractional luminosity of 11% in the 0.3-10 keV band. If this source is a black hole binary, it is possibly in the hard state.

Source 34. — The source sits at the north end of the NGC 247 disk, and was bright during the 2001 XMM-Newton observation with $\Gamma = 2.3_{-0.9}^{+1.5}$, $N_{\text{H}} = 1.9_{-0.8}^{+2.4} \times 10^{21}$ cm $^{-2}$, and $f_{\text{X}} = 2.0 \times 10^{-13}$ erg cm $^{-2}$ s $^{-1}$ in the 0.3-10 keV band, or $L_{\text{X}} = 4.6 \times 10^{38}$ erg s $^{-1}$ corrected for absorption. However, it became faint in the 2009 XMM-Newton observation, with a flux of 3.4×10^{-14} erg cm $^{-2}$ s $^{-1}$ in the 0.3-10 keV band, six times dimmer than in 2001. It is possibly source 3 in Fabbiano et al. (1992) from Einstein observations and source 1 in Read et al. (1997) from ROSAT observations. The ROSAT observations revealed a luminosity of 1.7×10^{38} erg s $^{-1}$ corrected for Galactic absorption only (at 3.4 Mpc) in the 0.1-2 keV band, or 3×10^{38} erg s $^{-1}$ corrected for all absorption. The luminosity in the same band from the 2001 XMM-Newton observation is about 6×10^{38} erg s $^{-1}$.

There is no bright optical counterpart found at the X-ray position. However, the source is associated with a possible star forming region, seen in the ultraviolet image from the 2001 XMM-Newton observation, with diffuse emission and star clusters nearby. Therefore, the source is likely an X-ray binary in NGC 247, and is perhaps an accreting black hole.

Source 36. — This source could be source 3 in Read et al. (1997). The best-fitted column density is consistent with the Galactic value. Its flux estimated

from the 2001 XMM-Newton observation is consistent with that in 2009. In the X-ray image, the source seems to show extended features and may consist of multiple objects, which can only be resolved with future Chandra observations.

Source 61. — Its X-ray spectrum cannot be adequately fitted by a single power-law model, with $\chi^2/\text{dof} = 80.9/60$; adding a Gaussian absorption line significantly improves the fit with $\chi^2/\text{dof} = 58.1/57$. The absorption line has a central energy of 0.9 ± 0.1 keV and a width of $\sigma = 0.22_{-0.16}^{+0.28}$ keV with an optical depth of $0.29_{-0.19}^{+0.58}$. The equivalent width is calculated to be around 0.30 keV. Its observed flux in 2001 was about twice of that in 2009. There is a bright optical source with $B = 18.83$ and $R = 18.58$ within $2''$ of the X-ray position, and the X-ray to optical flux ratio is estimated to be -0.3 . As discussed above, this source is likely a background AGN. Due to the low absorption column density, the absorption line is likely produced intrinsic to the source. Similar absorption has been seen in AGN (Blustin et al. 2002).

Source 13. — This is the hardest source detected with XMM-Newton. It is obvious in the hard band (2-10 keV) but undetected in the soft band (0.3-2 keV), consistent with $N_{\text{H}} > 5 \times 10^{22}$ cm $^{-2}$ for a power-law spectrum with $\Gamma = 2$. The source lies about $7'$ west of the nucleus of NGC 247, and is likely a highly absorbed background AGN.

Sources 41, 50, 59, and 72. — These four sources are the softest besides the ULX and are only detected in the soft band (0.3-2 keV) with a hardness ratio around -0.9 , which is consistent with a spectrum with a blackbody temperature < 0.4 keV or a power-law photon index $\Gamma > 2.5$, assuming Galactic absorption. Sources 41 and 72 are outside of the D25 ellipse of NGC 247, but sources 50 and 59 are inside. Their X-ray luminosities are about $10^{36} - 10^{37}$ erg s $^{-1}$. These sources do not appear to have bright optical counterparts. They could be canonical supersoft sources that are powered by nuclear burning on the surface of white dwarfs, or high redshift AGN.

Facility: XMM-Newton

REFERENCES

- Begelman, M. C. 2002, ApJ, 568, L97
 Belczynski, K., Bulik, T., Fryer, C. L., Ruiter, A., Valsecchi, F., Vink, J. S., Hurley, J. R. 2010, MNRAS, 714, 1217
 Blustin, A. J., Branduardi-Raymont, G., Behar, E., Kaastra, J. S., Kahn, S. M., Page, M. J., Sako, M., & Steenbrugge, K. C. 2002, A&A, 392, 453
 Brandt, W. N., & Hasinger, G. 2005, ARA&A, 43, 827
 Carpano, S., Pollock, A. M. T., King, A. R., Wilms, J., & Ehle, M. 2007, A&A, 471, L55
 Colbert, E. J. M., & Mushotzky, R. F. 1999, ApJ, 519, 89
 Davidge, T. J. 2006, ApJ, 641, 822
 Ebisuzaki, T., Makino, J., Tsuru, T. G., Funato, Y., Portegies Zwart, S., Hut, P., McMillan, S., Matsushita, S., Matsumoto, H., & Kawabe, R. 2001, ApJ, 562, L19
 Elvis, M., Fiore, F., Giommi, P., & Padovani, P. 1997, MNRAS, 291, L49
 Fabbiano, G., Kim, D.-W., & Trinchieri, G. 1992, ApJS, 80, 531
 Fabbiano, G., King, A. R., Zezas, A., Ponman, T. J., Rots, A., & Schweizer, François 2003, ApJ, 591, 843
 Farrell, S. A., Webb, N. A., Barret, D., Godet, O., Rodrigues, J. M. 2009, Nature, 460, 73
 Feng, H., & Kaaret, P. 2005, ApJ, 633, 1052
 Feng, H., & Kaaret, P. 2007, ApJ, 660, L113
 Feng, H., & Kaaret, P. 2009, ApJ, 696, 1712
 Feng, H., & Kaaret, P. 2010, ApJ, 712, L169
 Ferguson, A. M. N., Wyse, R. F. F., Gallagher, J. S., III, & Hunter, D. A. 1996, AJ, 111, 2265
 Gladstone, J. C., Roberts, T. P., & Done, C. 2009, MNRAS, 397, 1836
 Gieren, W., et al. 2009, ApJ, 700, 1141
 Grimm, H. J., Gilfanov, M., & Sunyaev, R. 2003, MNRAS, 339, 793
 González-Martín, O., Papadakis, I., Reig, P., & Zezas, A. 2011, A&A, 526, A132
 Isobe, N., Kubota, A., Makishima, K., Gandhi, P., Griffiths, R. E., Dewangan, G. C., Itoh, T., & Mizuno, T. 2008, PASJ, 60, S241
 Jin, J., Feng, H., & Kaaret, P. 2010, ApJ, 716, 181

- Kaaret, P., Prestwich, A. H., Zezas, A., Murray, S. S., Kim, D.-W., Kilgard, R. E., Schlegel, E. M., Ward, M. J. 2001, *MNRAS*, 321, L29
- Kajava, J. J. E., & Poutanen, J. 2009, *MNRAS*, 398, 1450
- Kalberla, P. M. W., Burton, W. B., Hartmann, D., Arnal, E. M., Bajaja, E., Morras, R., & Pöppel, W. G. L. 2005, *A&A*, 440, 775
- Kim, D. W., & Fabbiano, G. 2004, *ApJ*, 611, 846
- Kong, A. K. H., & Di Stefano, R. 2005, 632, L107
- Kong, A. K. H., Di Stefano, R., & Yuan, F. 2004, 617, L49
- Leahy, D. A., Darbro, W., Elsner, R. F., Weisskopf, M. C., Sutherland, P. G., Sutherland, P. G., Kahn, S., & Grindlay, J. E. 1983, *ApJ*, 266, 160
- Lira, P., Lawrence, A. & Johnson, R. A. 2000, *MNRAS*, 319, 17
- Liu, J. 2008, *ApJS*, 177, 181
- Maccacaro, T., et al. 1982, *ApJ*, 253, 504
- Maccacaro, T., Gioia, I. M., Wolter, A., Zamorani, G., & Stocke, J. T. 1988, *ApJ*, 326, 680
- Makishima, K., et al. 2000, *ApJ*, 535, 632
- Margon, B., Downes, R. A., & Chanan, G. A. 1985, *ApJS*, 59, 23
- McClintock, J. E., & Remillard, R. A. 2006, in *Compact Stellar X-ray sources*, ed. W. H. G. Lewin & M. van der Klis (Cambridge: Cambridge Univ. Press), 157
- Mukai, K., Pence, W. D., Snowden, S. L., & Kuntz, K. D. 2003, *ApJ*, 582: 184
- Mukai, K., Still, M., Gorbet, R. H. D., Kuntz, K. D., & Barnard, R. 2005, *ApJ*, 634, 1085
- Ohsuga, K., Mori, M., Nakamoto, T., & Mineshige, S. 2005, *ApJ*, 628, 368
- Pence, W. D., Snowden, S. L., Mukai, K., & Kuntz, K. D. 2001, *ApJ*, 561: 189
- Poutanen, J., Lipunova, G., Fabrika, S., Butkevich, A. G., & Abolmasov, P. 2007, *MNRAS*, 377, 1187
- Protassov, R., van Dyk, D. A., Connors, A., Kashyap, V. L., & Siemiginowska, A. 2002, *ApJ*, 571, 545
- Rao, F., Feng, H., & Kaaret, P. 2010, *ApJ*, 722, 620
- Read, A. M., Ponman, T. J., & Strickland, D. K. 1997, *MNRAS*, 286, 626
- Reeves, J. N., O'Brien, P. T., & Ward, M. J. 2003, *ApJ*, 593, L65
- Remillard, R. A., & McClintock, J. E. 2006, *ARA&A*, 44, 49
- Roberts, T. P., Gladstone, J. C., Goulding, A. D., Swinbank, A. M., Ward, M. J., Goad, M. R., & Levan, A. J. 2010, arXiv:1011.2155
- Soria, R., Baldi, A., Risaliti, G., Fabbiano, G., King, A., La Parola, V., & Zezas, A. 2007, *MNRAS*, 379, 1313
- Soria, R., & Ghosh, K. K. 2009, *ApJ*, 696, 287
- Starrfield, S., Timmes, F. X., Hix, W. R., Sion, E. M., Sparks, W. M., & Dwyer, S. J. 2004, *ApJ*, 612, L53
- Stobbart, A.-M., Roberts, T. P., & Wilms, J. 2006, *MNRAS*, 368, 397
- Stocke, J. T., Morris, S. L., Gioia, I. M., Maccacaro, T., Schild, R., Wolter, A., Fleming, T. A., & Henry, J. P. 1991, *ApJS*, 76, 813
- Swartz, D. A., Ghosh, K. K., Suleimanov, V., Tennant, A. F., & Wu, K. 2002, *ApJ*, 574, 382
- Volonteri, M. 2010, *Astron. Astrophys. Rev.*, 18, 279
- Watarai, K.-Y., Mizuno, T., & Mineshige, S. 2001, *ApJ*, 549, L77
- Winter, L. M., Mushotzky, R. F., & Reynolds, C. S. 2006, *ApJ*, 649, 730
- Zang, Z., Warwick, R. S., & Meurs, E. J. A. 1997, *Irish Astr. J.*, 24, 45
- Zhou, X.-L., Zhang, S.-N., Wang, D.-X., & Zhu, L. 2010, *ApJ*, 710, 16

TABLE 1
THE XMM-NEWTON SOURCE LIST OF NGC 247.

No.	IAU name (XMMU)	R.A. (J2000.0)	decl. (J2000.0)	err (")	flux1 (0.3-2 keV)	flux2 (2-10 keV)	hardness	like.	D25	note
(1)	(2)	(3)	(4)	(5)	(6)	(7)	(8)	(9)	(10)	(11)
1	J004609.2-204504	00 46 09.29	-20 45 04.9	2.21	0.050 ± 0.014	0.09 ± 0.07	-0.5 ± 0.3	13.7	no	
2	J004617.0-204151	00 46 17.00	-20 41 51.8	1.44	0.021 ± 0.013	0.27 ± 0.08	0.6 ± 0.3	15.9	no	
3	J004623.0-204740	00 46 23.02	-20 47 40.3	1.02	0.066 ± 0.012	0.21 ± 0.07	-0.26 ± 0.18	73.5	no	
4	J004628.7-205005	00 46 28.73	-20 50 05.2	0.78	0.22 ± 0.02	0.26 ± 0.06	-0.54 ± 0.09	195.4	no	O
5	J004631.1-203959	00 46 31.14	-20 39 59.1	1.89	0.052 ± 0.015	0.25 ± 0.08	0.1 ± 0.2	17.2	no	
6	J004632.1-205044	00 46 32.11	-20 50 44.2	1.85	0.032 ± 0.009	0.13 ± 0.06	-0.2 ± 0.3	18.6	no	
7	J004633.1-205457	00 46 33.16	-20 54 57.3	1.40	0.065 ± 0.014	0.06 ± 0.04	-0.7 ± 0.2	20.1	no	
8	J004634.1-205411	00 46 34.15	-20 54 11.2	0.93	0.042 ± 0.009	0.08 ± 0.05	-0.5 ± 0.2	51.1	no	
9	J004635.1-203529	00 46 35.17	-20 35 29.2	1.25	0.17 ± 0.04	0.37 ± 0.16	-0.2 ± 0.2	42.3	no	
10	J004635.2-203648	00 46 35.23	-20 36 48.2	1.43	0.086 ± 0.018	0.35 ± 0.12	-0.10 ± 0.19	40.6	no	
11	J004636.2-210018	00 46 36.29	-21 00 18.7	1.00	0.22 ± 0.03	0.11 ± 0.07	-0.75 ± 0.14	99.8	no	O
12	J004638.0-203609	00 46 38.04	-20 36 09.6	1.62	0.079 ± 0.018	0.08 ± 0.09	-0.7 ± 0.3	32.5	no	
13	J004639.6-204533	00 46 39.67	-20 45 33.6	1.05	< 0.0047	0.26 ± 0.06	> 0.79	40.4	no	
14	J004642.6-204507	00 46 42.64	-20 45 07.5	1.49	0.032 ± 0.008	0.05 ± 0.04	-0.6 ± 0.3	19.4	no	
15	J004645.8-210030	00 46 45.85	-21 00 30.6	1.78	0.084 ± 0.019	0.19 ± 0.08	-0.2 ± 0.2	21.7	no	
16	J004646.3-204742	00 46 46.39	-20 47 42.7	0.51	0.112 ± 0.012	0.34 ± 0.06	-0.30 ± 0.09	327.2	no	O
17	J004646.9-203658	00 46 46.92	-20 36 58.0	1.56	0.063 ± 0.015	0.13 ± 0.07	-0.4 ± 0.3	19.8	no	
18	J004647.2-203628	00 46 47.23	-20 36 28.1	1.78	0.070 ± 0.016	0.14 ± 0.08	-0.4 ± 0.3	22.1	no	
19	J004647.7-203837	00 46 47.72	-20 38 37.3	0.65	0.23 ± 0.02	0.37 ± 0.09	-0.52 ± 0.09	333.1	no	O
20	J004648.8-205247	00 46 48.85	-20 52 47.0	1.20	0.053 ± 0.009	0.07 ± 0.04	-0.60 ± 0.19	60.6	no	
21	J004650.4-203854	00 46 50.47	-20 38 54.0	1.76	0.042 ± 0.012	0.05 ± 0.06	-0.6 ± 0.4	17.4	no	
22	J004651.8-204328	00 46 51.82	-20 43 28.5	0.14	2.26 ± 0.05	2.62 ± 0.14	-0.655 ± 0.016	14105.3	no	QSO
23	J004654.6-204129	00 46 54.63	-20 41 29.4	0.78	0.086 ± 0.012	0.12 ± 0.05	-0.59 ± 0.15	92.5	yes	O
24	J004654.8-204100	00 46 54.87	-20 41 00.9	0.56	0.196 ± 0.018	0.42 ± 0.08	-0.43 ± 0.08	381.1	yes	
25	J004655.7-203407	00 46 55.74	-20 34 07.6	1.55	0.084 ± 0.018	0.12 ± 0.12	-0.5 ± 0.3	19.5	no	
26	J004655.9-205248	00 46 55.92	-20 52 48.4	1.48	0.026 ± 0.008	0.11 ± 0.04	0.0 ± 0.2	18.1	no	
27	J004656.4-205611	00 46 56.43	-20 56 11.9	1.34	0.053 ± 0.010	0.19 ± 0.06	-0.20 ± 0.18	35.7	no	
28	J004659.3-204538	00 46 59.38	-20 45 38.8	0.26	0.336 ± 0.019	1.06 ± 0.09	-0.28 ± 0.05	1796.1	yes	
29	J004659.7-204227	00 46 59.70	-20 42 27.3	1.34	0.063 ± 0.010	0.03 ± 0.04	-0.84 ± 0.17	38.7	yes	
30	J004700.5-203359	00 47 00.55	-20 33 59.7	3.09	0.05 ± 0.02	0.35 ± 0.11	0.3 ± 0.2	10.9	no	
31	J004701.9-205450	00 47 01.98	-20 54 50.8	1.62	0.026 ± 0.007	0.08 ± 0.04	-0.3 ± 0.3	23.2	no	
32	J004702.7-205302	00 47 02.79	-20 53 02.9	1.97	0.032 ± 0.010	0.03 ± 0.03	-0.7 ± 0.3	14.7	yes	

TABLE 1 — *Continued*

No.	IAU name (XMMU)	R.A. (J2000.0)	decl. (J2000.0)	err ($''$)	flux1 (0.3-2 keV)	flux2 (2-10 keV)	hardness	like.	D25	note
(1)	(2)	(3)	(4)	(5)	(6)	(7)	(8)	(9)	(10)	(11)
33	J004703.2–204545	00 47 03.23	–20 45 45.9	1.12	0.042 ± 0.009	0.17 ± 0.04	-0.01 ± 0.18	56.2	yes	
34	J004703.2–203657	00 47 03.28	–20 36 57.9	1.64	0.034 ± 0.011	0.31 ± 0.09	0.3 ± 0.2	20.1	yes	
35	J004703.4–204321	00 47 03.44	–20 43 21.5	1.02	0.034 ± 0.009	0.21 ± 0.05	0.20 ± 0.18	42.7	yes	
36	J004703.6–204015	00 47 03.68	–20 40 15.6	0.42	0.43 ± 0.03	0.60 ± 0.09	-0.59 ± 0.05	1184.2	yes	
37	J004703.9–204743	00 47 03.90	–20 47 43.8	0.16	1.84 ± 0.04	0.13 ± 0.04	-0.975 ± 0.008	9827.5	yes	ULX
38	J004704.5–205812	00 47 04.57	–20 58 12.0	1.94	0.061 ± 0.019	0.23 ± 0.09	-0.0 ± 0.2	17.8	no	
39	J004705.9–205239	00 47 05.92	–20 52 39.4	0.75	0.071 ± 0.010	0.11 ± 0.04	-0.57 ± 0.14	152.1	yes	O
40	J004705.9–204152	00 47 05.94	–20 41 52.4	1.07	0.088 ± 0.013	0.13 ± 0.06	-0.57 ± 0.15	69.9	yes	
41	J004707.3–205749	00 47 07.38	–20 57 49.3	1.30	0.073 ± 0.013	< 0.04	< -0.78	51.4	no	
42	J004708.0–204346	00 47 08.01	–20 43 46.8	1.57	0.020 ± 0.008	0.13 ± 0.04	0.2 ± 0.3	10.4	yes	
43	J004709.0–205214	00 47 09.03	–20 52 14.7	0.73	0.077 ± 0.011	0.30 ± 0.06	-0.18 ± 0.12	172.1	yes	
44	J004709.1–204622	00 47 09.16	–20 46 22.8	1.10	0.060 ± 0.010	0.19 ± 0.04	-0.22 ± 0.13	56.1	yes	
45	J004710.0–204708	00 47 10.06	–20 47 08.4	0.34	0.237 ± 0.016	0.81 ± 0.08	-0.25 ± 0.05	1117.2	yes	
46	J004710.3–204343	00 47 10.32	–20 43 43.9	1.29	0.029 ± 0.008	0.07 ± 0.04	-0.4 ± 0.3	24.8	yes	
47	J004712.4–204219	00 47 12.48	–20 42 19.1	1.45	0.027 ± 0.009	0.10 ± 0.04	-0.2 ± 0.4	15.6	yes	
48	J004712.7–203837	00 47 12.74	–20 38 37.0	1.88	0.042 ± 0.011	0.15 ± 0.07	-0.2 ± 0.3	14.0	yes	O, I
49	J004713.7–205113	00 47 13.70	–20 51 13.4	1.15	0.033 ± 0.008	0.09 ± 0.04	-0.4 ± 0.2	45.1	yes	
50	J004715.1–204717	00 47 15.17	–20 47 17.3	0.96	0.059 ± 0.009	0.01 ± 0.02	-0.92 ± 0.11	66.3	yes	
51	J004715.9–205502	00 47 15.94	–20 55 02.5	0.75	0.161 ± 0.017	0.21 ± 0.06	-0.61 ± 0.10	235.8	yes	
52	J004716.5–204814	00 47 16.59	–20 48 14.4	0.85	0.047 ± 0.008	0.10 ± 0.04	-0.47 ± 0.17	84.1	yes	
53	J004716.6–203346	00 47 16.63	–20 33 46.4	1.09	0.056 ± 0.018	0.39 ± 0.14	0.2 ± 0.2	11.1	no	
54	J004717.9–205508	00 47 17.93	–20 55 08.6	0.99	0.111 ± 0.014	0.23 ± 0.06	-0.45 ± 0.12	97.5	yes	
55	J004718.5–204739	00 47 18.56	–20 47 39.8	0.90	0.072 ± 0.011	0.17 ± 0.04	-0.38 ± 0.15	64.2	yes	
56	J004719.7–205601	00 47 19.77	–20 56 01.3	1.90	0.032 ± 0.009	0.07 ± 0.05	-0.4 ± 0.3	11.8	no	
57	J004720.3–205248	00 47 20.32	–20 52 48.7	1.00	0.083 ± 0.012	0.06 ± 0.04	-0.78 ± 0.16	110.1	yes	O(2), I
58	J004721.0–204932	00 47 21.05	–20 49 32.3	1.32	0.038 ± 0.009	0.13 ± 0.04	-0.1 ± 0.2	25.0	yes	
59	J004721.4–205104	00 47 21.48	–20 51 04.1	1.80	0.021 ± 0.007	< 0.012	< -0.80	14.8	yes	
60	J004725.2–205442	00 47 25.23	–20 54 42.4	1.28	0.15 ± 0.03	0.13 ± 0.07	-0.64 ± 0.17	67.5	no	
61	J004727.3–204721	00 47 27.36	–20 47 21.6	0.28	0.58 ± 0.03	0.55 ± 0.08	-0.71 ± 0.04	2204.7	no	O
62	J004728.7–204301	00 47 28.76	–20 43 01.7	0.72	0.127 ± 0.016	0.21 ± 0.07	-0.54 ± 0.12	162.3	no	O
63	J004730.6–205434	00 47 30.64	–20 54 34.0	0.68	0.23 ± 0.03	0.56 ± 0.12	-0.23 ± 0.12	223.0	no	
64	J004733.5–204557	00 47 33.57	–20 45 57.5	1.16	0.035 ± 0.009	0.18 ± 0.06	-0.0 ± 0.2	27.4	no	
65	J004737.4–203648	00 47 37.49	–20 36 48.3	1.50	0.060 ± 0.017	0.39 ± 0.13	0.1 ± 0.2	25.3	no	O
66	J004740.7–204442	00 47 40.77	–20 44 42.5	1.87	0.040 ± 0.011	0.15 ± 0.08	-0.2 ± 0.3	15.9	no	
67	J004741.8–205231	00 47 41.84	–20 52 31.5	0.52	0.38 ± 0.03	0.79 ± 0.11	-0.30 ± 0.07	485.8	no	O(2)
68	J004743.4–204941	00 47 43.49	–20 49 41.4	0.68	0.178 ± 0.019	0.29 ± 0.08	-0.53 ± 0.11	230.5	no	
69	J004744.5–205321	00 47 44.53	–20 53 21.2	1.03	0.12 ± 0.02	0.24 ± 0.08	-0.31 ± 0.17	65.2	no	O
70	J004752.1–204053	00 47 52.19	–20 40 53.9	1.78	0.066 ± 0.017	0.12 ± 0.12	-0.5 ± 0.4	22.5	no	O
71	J004753.5–205435	00 47 53.55	–20 54 35.3	1.23	0.11 ± 0.02	0.09 ± 0.06	-0.5 ± 0.3	39.8	no	
72	J004759.1–205201	00 47 59.19	–20 52 01.2	2.02	0.068 ± 0.017	0.03 ± 0.06	-0.9 ± 0.3	11.7	no	
73	J004808.3–204553	00 48 08.39	–20 45 53.3	3.61	0.053 ± 0.019	0.53 ± 0.15	0.3 ± 0.2	13.7	no	
74	J004810.7–204818	00 48 10.75	–20 48 18.5	9.07	0.029 ± 0.016	0.57 ± 0.16	0.6 ± 0.2	11.2	no	
75	J004812.3–204755	00 48 12.30	–20 47 55.6	2.56	0.031 ± 0.016	0.54 ± 0.15	0.6 ± 0.2	12.4	no	

NOTE. — Col. (2-5): Source names, coordinates, and position errors. Col. (6-7): Absorbed fluxes in units of 10^{-13} erg cm^{-2} s^{-1} . Col. (8-10): Hardness ratios, detection likelihood, and whether or not the source is inside the D25 ellipse of NGC 247. Col. (11): ‘O’ denotes optical counterparts found in USNO-B1.0 with numbers, if more than one, shown in parentheses; ‘I’ denotes counterparts found in 2MASS. 90% upper bounds are quoted for non-detections.

TABLE 2
SPECTRAL PARAMETERS OF BRIGHT SOURCES IN NGC 247 FITTED WITH A
POWER-LAW MODEL.

No.	N_{H}	Γ	N_{PL}	f_{X}	L_{X}	χ^2/dof
4	$0.2^{+0.8}_{-0}$	$1.7^{+0.4}_{-0.3}$	$1.01^{+0.43}_{-0.17}$	$0.71^{+0.15}_{-0.22}$	$1.0^{+0.3}_{-0.2}$	8.7/10
16	$0.2^{+0.7}_{-0}$	$1.2^{+0.4}_{-0.3}$	$0.45^{+0.15}_{-0.08}$	$0.52^{+0.13}_{-0.16}$	$0.7^{+0.2}_{-0.2}$	20.8/17
19	$0.2^{+0.3}_{-0}$	$2.0^{+0.3}_{-0.3}$	$0.90^{+0.14}_{-0.12}$	$0.50^{+0.09}_{-0.14}$	$0.70^{+0.17}_{-0.14}$	18.3/15
22*	$0.27^{+0.17}_{-0.07}$	$2.10^{+0.13}_{-0.09}$	$17.4^{+2.1}_{-1.3}$	$4.3^{+0.3}_{-0.3}$	$2.26^{+0.12}_{-0.12} \times 10^6$	99.2/99
24	$1.9^{+1.1}_{-0.8}$	$2.3^{+0.6}_{-0.2}$	$1.4^{+1.0}_{-0.5}$	$0.41^{+0.16}_{-0.11}$	$1.0^{+0.8}_{-0.2}$	17.9/14
28	$0.20^{+0.08}_{-0}$	$1.27^{+0.10}_{-0.10}$	$1.42^{+0.10}_{-0.10}$	$1.55^{+0.13}_{-0.14}$	$2.16^{+0.20}_{-0.19}$	57.2/56
36	$0.2^{+0.2}_{-0}$	$1.69^{+0.14}_{-0.11}$	$2.07^{+0.22}_{-0.14}$	$1.43^{+0.15}_{-0.23}$	$2.0^{+0.3}_{-0.2}$	59.9/52
39	$0.2^{+0.8}_{-0}$	$1.5^{+0.6}_{-0.4}$	$0.34^{+0.19}_{-0.06}$	$0.30^{+0.11}_{-0.14}$	$0.42^{+0.16}_{-0.14}$	7.3/8
43	$3.9^{+2.6}_{-1.5}$	$1.9^{+0.3}_{-0.2}$	$0.8^{+0.9}_{-0.4}$	$0.34^{+0.12}_{-0.10}$	$0.71^{+0.42}_{-0.15}$	6.0/11
45	$1.5^{+0.9}_{-0.5}$	$1.66^{+0.16}_{-0.16}$	$1.7^{+0.4}_{-0.3}$	$1.02^{+0.15}_{-0.14}$	$1.72^{+0.17}_{-0.17}$	46.8/46
51	$1.2^{+0.9}_{-0.8}$	$1.9^{+0.3}_{-0.5}$	$0.8^{+0.5}_{-0.3}$	$0.37^{+0.15}_{-0.11}$	$0.67^{+0.23}_{-0.13}$	7.6/8
61	$0.20^{+0.06}_{-0}$	$2.13^{+0.13}_{-0.13}$	$2.16^{+0.13}_{-0.13}$	$1.13^{+0.09}_{-0.08}$	$1.58^{+0.20}_{-0.14}$	80.9/60
62	$0.2^{+0.5}_{-0}$	$1.8^{+0.5}_{-0.4}$	$0.59^{+0.15}_{-0.10}$	$0.38^{+0.11}_{-0.15}$	$0.51^{+0.20}_{-0.09}$	12.2/12
63	$2.2^{+1.5}_{-1.3}$	$1.8^{+0.4}_{-0.2}$	$1.4^{+0.9}_{-0.5}$	$0.7^{+0.3}_{-0.2}$	$1.3^{+0.3}_{-0.2}$	7.2/13

TABLE 2 — *Continued*

No.	N_{H}	Γ	N_{PL}	f_{X}	L_{X}	χ^2/dof
67	$0.6^{+1.0}_{-0.4}$	$1.7^{+0.4}_{-0.4}$	$1.8^{+0.9}_{-0.5}$	$1.2^{+0.3}_{-0.3}$	$1.8^{+0.4}_{-0.3}$	14.1/13
68	$0.2^{+0.8}_{-0}$	$1.8^{+0.6}_{-0.3}$	$0.78^{+0.36}_{-0.11}$	$0.49^{+0.15}_{-0.18}$	$0.70^{+0.21}_{-0.17}$	19.3/14

NOTE. — N_{H} is the absorption column density in 10^{21} cm^{-2} . Γ is the power-law photon index. N_{PL} is the power-law normalization at 1 keV in units of $10^{-5} \text{ photons keV}^{-1} \text{ cm}^{-2} \text{ s}^{-1}$. f_{X} is the observed flux in 0.3-10 keV in units of $10^{-13} \text{ erg cm}^{-2} \text{ s}^{-1}$. L_{X} is the unabsorbed luminosity in 0.3-10 keV in units of $10^{38} \text{ erg s}^{-1}$. Errors are quoted at 90% confidence level.

* A redshifted power-law model with $z = 0.38$ is used, and a luminosity distance of 2.0 Gpc assuming $H_0 = 70 \text{ km s}^{-1} \text{ Mpc}^{-1}$ is adopted.

TABLE 3
SPECTRAL PARAMETERS OF NGC 247 ULX.

	N_{H}	thermal		power-law		absorption			f_{X}	L_{X}	χ^2/dof
		kT	R	Γ	N_{PL}	E	τ	σ			
a1	3.2*	$0.117^{+0.003}_{-0.003}$	$1.34^{+0.12}_{-0.13}$	$1.6^{+0.6}_{-0.7}$	$0.5^{+0.5}_{-0.3}$	$1.75^{+0.18}_{-0.15}$	$2.92^{+0.16}_{-0.16}$	88.0/43
a2	$3.2^{+0.7}_{-0.7}$	$0.13^{+0.02}_{-0.02}$	$0.9^{+1.3}_{-0.5}$	$2.5^{+1.4}_{-1.0}$	$1.7^{+3.3}_{-1.2}$	$1.02^{+0.02}_{-0.03}$	$1.4^{+0.5}_{-0.5}$...	$1.71^{+0.17}_{-0.13}$	$2.7^{+3.4}_{-1.3}$	36.8/40
a3	$3.5^{+0.9}_{-0.8}$	$0.123^{+0.022}_{-0.012}$	$1.3^{+1.2}_{-0.4}$	$2.0^{+1.1}_{-1.0}$	$0.9^{+1.3}_{-0.6}$	$1.16^{+0.05}_{-0.03}$	$0.26^{+0.08}_{-0.08}$	$0.08^{+0.04}_{-0.03}$	$1.74^{+0.18}_{-0.14}$	$3.4^{+4.0}_{-1.6}$	37.0/39
b1	2.7*	$0.103^{+0.003}_{-0.002}$	$1.35^{+0.07}_{-0.11}$	$1.6^{+0.6}_{-0.7}$	$0.6^{+0.5}_{-0.3}$	$1.76^{+0.18}_{-0.15}$	$1.74^{+0.09}_{-0.09}$	81.5/43
b2	$2.7^{+1.0}_{-0.7}$	$0.112^{+0.016}_{-0.017}$	$1.0^{+1.3}_{-0.5}$	$2.7^{+2.2}_{-1.0}$	$2.0^{+7.5}_{-1.4}$	$1.02^{+0.03}_{-0.03}$	$1.3^{+0.5}_{-0.4}$...	$1.70^{+0.17}_{-0.14}$	$1.6^{+2.9}_{-0.8}$	39.0/40
b3	$2.9^{+0.9}_{-0.7}$	$0.109^{+0.017}_{-0.013}$	$1.2^{+1.2}_{-0.5}$	$2.1^{+1.2}_{-0.9}$	$1.0^{+1.4}_{-0.6}$	$1.15^{+0.04}_{-0.03}$	$0.23^{+0.07}_{-0.08}$	$0.08^{+0.04}_{-0.03}$	$1.74^{+0.18}_{-0.14}$	$1.9^{+1.7}_{-0.9}$	38.9/39

NOTE. — XSPEC models **a1**: wabs * (diskbb + powerlaw); **a2**: wabs * edge * (diskbb + powerlaw); **a3**: wabs * gabs * (diskbb + powerlaw); **b1**: wabs * (bbodyrad + powerlaw); **b2**: wabs * edge * (bbodyrad + powerlaw); **b3**: wabs * gabs * (bbodyrad + powerlaw). N_{H} is the absorption column density in 10^{21} cm^{-2} . kT and R are temperature in keV and face-on radius in 10^4 km of the thermal component, respectively; for the diskbb model, they correspond to the values at the innermost disk. Γ is the power-law photon index. N_{PL} is the power-law normalization at 1 keV in units of $10^{-5} \text{ photons keV}^{-1} \text{ cm}^{-2} \text{ s}^{-1}$. E and τ are energy in keV and optical depth of the local absorption component, respectively, and σ is the width of the Gaussian absorption in keV. f_{X} is the observed flux in 0.3-10 keV in units of $10^{-13} \text{ erg cm}^{-2} \text{ s}^{-1}$. L_{X} is the unabsorbed luminosity in 0.3-10 keV in units of $10^{39} \text{ erg s}^{-1}$. Errors are quoted at 90% confidence level.

* Fixed at the value obtained from the best-fit model.

TABLE 4
COMPARISON OF THE THERMAL EMISSION COMPONENT IN ULXs.

	Temperature	Fraction	Fast Variability	$L \propto T^4$
NGC 247 ULX	low ($\sim 0.1 \text{ keV}$)	major	high	unknown
other supersoft ULXs	low ($\sim 0.1 \text{ keV}$)	major	high	no
M82 X41.4+60 during outburst ^a	high ($\sim 1 \text{ keV}$)	major	low	yes
other hot ULXs	high ($\sim 1 \text{ keV}$)	major	unknown	maybe ^b
soft excesses in ULXs	low (0.1-0.4 keV)	minor	weak ^c	rare ^d

NOTE. — Temperature is the typical temperature of the thermal emission component found in the X-ray spectrum. Fraction is ‘major’ if the thermal emission component produces more than 60% of the total X-ray flux. Fast Variability is ‘low’ if the variability of the thermal emission component is consistent with that of white noise. The last column indicates if the luminosity varies as the fourth power of the temperature of the thermal emission component.

^a when it is in the thermal dominant state (Feng & Kaaret 2010).

^b possibly seen in M82 X37.8+54 (Jin et al. 2010), Suzaku J1305–4931 (Isobe et al. 2008), and NGC 253 X-2 (Kajava & Poutanen 2009)

^c A few ULXs show strong variabilities, e.g., NGC 6946 X-1 (Rao et al. 2010), M82 X41.4+60 in the low state (Feng & Kaaret 2010). However, their variabilities are mainly in the hard band.

^d possibly yes in NGC 5204 X-1 (Feng & Kaaret 2009), but definitely inconsistent in NGC 1313 X-2 (Feng & Kaaret 2007) and IC 342 X-1 (Feng & Kaaret 2009).